POLITECNICO MILANO 1863

SCUOLA DI INGEGNERIA INDUSTRIALE E DELL'INFORMAZIONE

Executive Summary of the Thesis

Meanline Design and Analysis of a Supersonic Centrifugal Turbine for Rotating Detonation Engines

Laurea Magistrale in Mechanical Engineering - Ingegneria Meccanica

Author: Rubens Zottino

Advisor: Prof. Paolo Gaetani

Co-advisor: Dr. Noraiz Mushtaq

Academic year: 2025-2026

---

1. Introduction

The continuous development of the energy market makes it essential to research innovative technologies capable of meeting demand in the most efficient and sustainable way possible. In the context of gas turbines, it has been demonstrated that adopting thermodynamic cycles alternative to the Joule–Brayton one can lead to efficiency increases of up to 25% [1]. Among these, significant confidence has been placed in pressure-gain systems, with the Rotating Detonation Engine (RDE) standing out in particular. This device requires an innovative supersonic inlet turbine capable of extracting high amounts of work without penalizing the overall system performance. A fully radial centrifugal turbine, developed entirely in the radial direction, is particularly suited, allowing easy integration with future non-annular RDE combustors. The increase in cross-sectional area along the meridional coordinate makes this type of machine strongly accelerating, allowing the blade channel starting limits to be satisfied more easily. The feasibility of such turbine can be initially assessed using meanline (ML) analysis, providing insight into its potential performance for supersonic RDE applications.

2. Design Methodology

2.1. Meanline Code

The code is based on a 1D formulation along the mean streamline, where the conservation equations of mass, momentum, and energy are solved together with appropriate loss correlations. The input parameters include the thermodynamic conditions at the stator inlet and the machine geometry (radial development, chord length, and leading/trailing edge (LE/TE) thickness). In order to determine the flow properties in each turbine section (see Figure 1) without overconstraining the problem, two non-dimensional parameters are introduced: the flow coefficient φ and the work coefficient λ, defined as:

$$\varphi = V_{1m}/U_2 \tag{1}$$

$$\lambda = l_{eu}/U_2^2 \tag{2}$$

The flow coefficient constrains the stator deflection by imposing the meridional velocity component at stator outlet, whereas the work coefficient defines the extracted work through the tangential velocity component at rotor outlet. Within the stator–rotor gap (SRG), a free-vortex isentropic condition is assumed. Aerodynamic losses are modeled according to the losses breakdown (LB) approach, whereby the total dissipation is expressed as the sum of independent contributions associated with specific physical mechanisms. The analysis focuses on profile losses and shock losses, while endwall and tip-clearance effects are neglected, consistently with the blade-to-blade nature of the ML approach. Profile losses are evaluated using the Stewart method [2], based on Stratford–Beavers boundary layer parameters [3]. Although originally developed for axial cascades, the model has been adapted to the centrifugal configuration, acknowledging the associated approximation. Shock losses account for the bow shock forming upstream of the LE and its first reflection inside the channel. The bow shock shape is described through the Moeckel method [4], while the reflected shock is modeled using the oblique shock relations. Entropy generation is locally computed through the jump conditions and integrated along the channel. Since no dedicated blade design tool is embedded in the code, only the camber lines are defined using Bézier curves, imposing passage points, inlet/outlet flow angles, and blade chord.

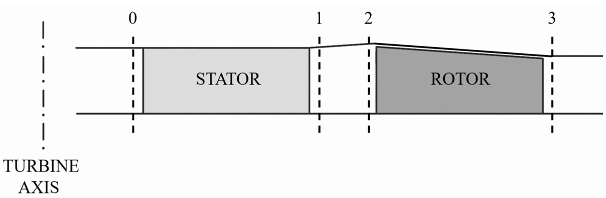

Figure 1: Turbine configuration and ML nomenclature.

2.2. Smith Maps

The solution field was mapped using Smith charts (φ–λ), varying non-dimensional ratios representative of the machine's scale and the stage inlet Mach number. During this process, particular care was taken to respect all fluid-dynamic constraints associated with the supersonic flow, such as the Kantrowitz limits and the formation of collective shocks ahead of the blade row [5]. The occurrence of the latter phenomenon was assessed by locating the intersection point of two consecutive bow shocks and verifying that its meridional coordinate remained within the blade channel. Figure 2 shows an example of one of the efficiency Smith charts obtained. The maps were generated neglecting reflected shock waves, as these are highly sensitive to the local blade geometry. Their inclusion would have introduced steep gradients in the represented fields, reducing readability and making the qualitative analysis of the trends under investigation more complex.

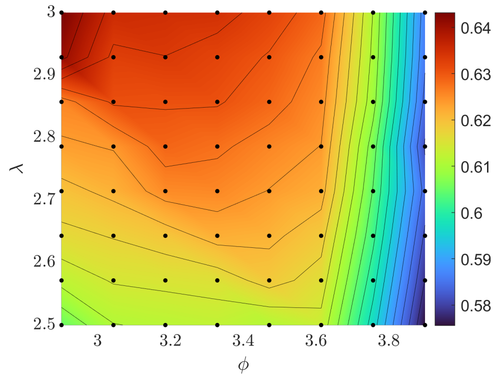

Figure 2: Efficiency Smith chart for $M_0 = 2$, $r_1/r_0 = 1.8$ and $r_3/r_2 = 1.4$.

2.3. CFD

In order to validate the results from the ML code and to further investigate the aerodynamic aspects of the turbine, several CFD analyses were performed using ANSYS CFX. The workflow for the simulations starts with mesh generation, followed by the specification of boundary conditions (BC), selection of solver parameters, and post-processing.

2.3.1 Mesh Generation via turboGrid

The mesh for the various components was generated using turboGrid, refining the discretization until grid independence was achieved. The blade geometry was created with BladeGen, since the meanline code does not integrate a design tool. This software allows assigning the coordinates of the blade LE and TE, as well as the distribution of geometric angles and thickness along the chord. The latter, however, cannot be set a priori to avoid over-constraining the problem, but is determined as a result by BladeGen. After fixing the blade inlet and outlet angles, several configurations were tested to identify the optimal aerodynamic loading, as shown in Figure 3. Subsequently, selected ML input parameters, including the chord length, were modified to better match the CFD configuration. Nevertheless, small differences persist between the two cases, mainly due to minor inaccuracies in the imposed boundary conditions.

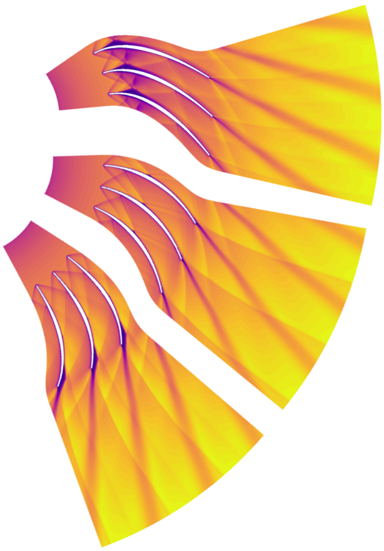

Figure 3: Blade profiles: top: front-loaded; center: best-performing; bottom: back-loaded.

2.3.2 Initialization via CFX–Pre

The problem was initialized using CFX–Pre. Here, the BC on each surface/interface generated by turboGrid and the initial conditions inside the domain are defined. A no-slip condition was applied on the blade surfaces, while a free-slip condition was imposed on the hub surfaces. The latter choice is essential to eliminate the contribution of endwall losses and to analyze a case physically analogous to the meanline model. Additionally, this assumption allows the use of two-dimensional simulations in the case of a blade row with constant height (stator). The common practice in CFD is to generate a mesh that extends along the meridional coordinate both upstream and downstream of the blade, where the flow properties vary due to the centrifugal configuration. Although the desired flow conditions are defined at the blade LE, the BC must be applied at the domain extremities. Therefore, it is necessary to derive the BC from the theoretical values evaluated along the meanline. To do this, the free-vortex isentropic flow assumption was adopted. To reduce the inaccuracy introduced by this approach, the domain should not extend too far upstream of the LE. Consequently, the meridional extension upstream of the LE is smaller than that commonly used in CFD simulations, being 0.5 chords for the stator and 0.2 chords for the rotor. The initialization phase concludes by assigning the properties of the working fluid and selecting the solver settings.

2.3.3 Post-Processing via CFD–Post

The CFD results were post-processed using a mass-flow averaging procedure applied on surfaces defined at the LE and TE of both stator and rotor. Regarding the loss evaluation, a different methodology was adopted. In order to account also for the contribution associated with flow mixing, entropy generation was computed on a surface located downstream of the TE, at a distance such that the flow could be considered fully mixed. This distance was determined on a case-by-case basis by analyzing the evolution of entropy generation along the streamwise coordinate and identifying the location at which it reaches a plateau (as shown in Figure 4).

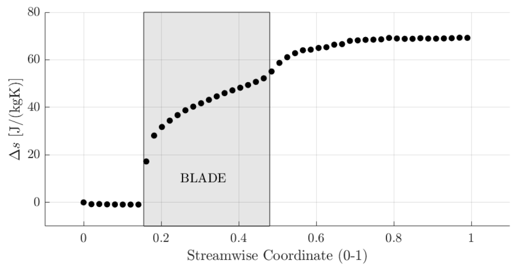

Figure 4: Mass-flow-averaged streamwise entropy production (stator, design point).

In the stage simulations, the stator and rotor domains were coupled through a mixing plane (MP). This approach performs a circumferential averaging of the flow properties at the stator outlet, enabling fully steady-state simulations. Although it is widely adopted due to its reduced computational cost, the use of a MP inevitably introduces a contribution of numerical entropy, physically associated with the mixing process of a flow that is non-uniform in the tangential direction. In order to quantify this contribution and to highlight the operational limits and critical aspects of the ML code, the following operating conditions were deliberately selected:

- **A)** Stator and rotor at the design point simulated separately (decoupled configuration);
- **B)** Stator and rotor at the design point in stage configuration (coupled via MP);

C) An operating point close to the region where the occurrence of collective shock is expected;

D) An operating point aimed at demonstrating the limitations of the ML model in estimating shock losses through the Moeckel method.

3. Results

3.1. Parametric Analysis

The parametric analysis presented in Section 2.2 shows that, for small geometries, low φ, and high λ, the formation of collective shocks on the rotor represents the most restrictive constraint, while efficiency increases with the work extracted. Increasing the rotor deflection therefore leads to improved performance, provided that the limits imposed by the Kantrowitz criterion and the onset of collective shocks are satisfied. This highlights the need for a careful assessment of the SRG, in which φ governs these phenomena through an increase in the Mach number and a reduction in the tangential velocity component. Moreover, the work extractable from the turbine increases with the enlargement of the rotor exit flow area, suggesting that the absence of a flaring angle may be advantageous. However, this configuration would result in higher outlet Mach number and less effective flow management downstream of the machine. With regard to the influence of the inlet Mach number, the standard configuration ($M_0 = 2$) proves to be the most efficient. A reduction in M_0 worsens the starting conditions and promotes the formation of collective shocks, whereas an increase leads to greater losses associated with shock waves. Based on the above results, the design point was selected on the map in Figure 2 at $\varphi = 3.5$ and $\lambda = 2.8$.

3.2. Validation of the design point

Table 1 reports the results obtained with the ML model for the design case and for CFD cases A and B. The main flow-field variables are well predicted by the ML code, with only minor discrepancies attributable to flow angle deviation. More pronounced differences emerge in the performance assessment: the stage simulation with a MP penalizes efficiency compared to the uncoupled cases, in which the rotor does not directly experience effects such as deviation, incidence, wake interaction, and the shock structure downstream of the stator.

Metric	Unit	*ML*	*CFD*$_A$	*CFD*$_B$
η_{tt}	%	56.68	54.52	51.57
l_{eu}	kJ/kg	357.1	331.5	325.3
M_1	-	2.077	2.071	2.071
M_{w2}	-	1.921	1.920	1.903
M_3	-	1.646	1.544	1.505
α_1	deg	42.63	41.60	41.57
β_2	deg	28.24	28.32	27.75
α_3	deg	2.260	4.176	4.141

Table 1: Comparison between the ML design configuration and CFD cases A and B.

However, the most significant deviation arises from the losses introduced at the MP, as shown in Table 2. The quantities with the suffix MP are evaluated at the the interface between stator and rotor domains, whereas those without the superscript exclude the entropy production occurring at that location, being computed immediately upstream (for the stator) or downstream (for the rotor). The entropy increase associated with the MP amounts to approximately 25.6 J/kgK, leading to a reduction in total pressure at the rotor inlet and a consequent penalty in work extraction in the coupled case.

Location	Unit	Value
Stator	J/kgK	56.30
Rotor	J/kgK	74.86
Stage	J/kgK	131.2
Stator MP	J/kgK	81.88
Rotor MP	J/kgK	74.91
Stage MP	J/kgK	156.8

Table 2: Entropy production across each component in CFD case B.

3.3. Model Limitations: Operating near Collective Shock Formation

In case C, the operating point is located near the region where a collective shock forms on the rotor. Consequently, the performance is significantly overestimated by the ML code. This occurs because the 1D code is unable to capture all the shock phenomena present in reality, such as Mach phenomena and the lambda shock observed on the pressure side of the LE of the rotor row (Figure 5, right side). From the results reported in Table 3, it is clear that the discrepancy between the ML code and CFD results is solely due to these shock phenomena and work reduction, as the entropy generation and the downstream properties of the stator are accurately predicted by the model. These results demonstrate that the selection of the operating point using a ML code must be carried out with caution and a conservative approach.

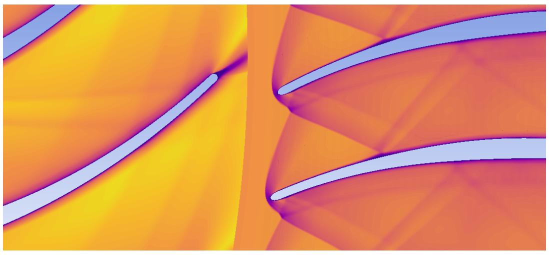

Figure 5: Mach contours showing Mach phenomena and lambda shocks in the case C rotor.

Metric	Unit	ML_C	CFD_C
η_{tt}	%	55.32	33.96
l_{eu}	kJ/kg	324.0	293.7
$\Delta s_{tot,MP}$	J/kgK	127.88	167.04
Δs_{stator}	J/kgK	71.97	70.41
Δs_{rotor}	J/kgK	55.91	72.97
M_1	-	2.020	2.010
M_{w2}	-	1.881	1.823
M_3	-	1.661	1.576
α_1	deg	44.59	42.84
β_2	deg	29.59	29.04
α_3	deg	5.520	7.072

Table 3: Comparison between ML and CFD results for case C. The entropy production in the stator and rotor is evaluated excluding the contribution from the mixing plane, which is, however, included in the assessment of the total entropy production (MP).

3.4. Model Limitations: Shock-Loss Estimation via Moeckel Method

Analyzing the results in Table 4, discrepancies are observed between the entropy values predicted by the ML code and those of CFD. These differences are due to the limited ability of the 1D code to accurately predict shock losses. As mentioned in Section 2.1, the shock wave pattern within the channel was evaluated only along the camber line, since the ML code does not include a tool for blade design. The neglect of blade thickness can lead, as shown in Figure 6, to the absence of bow shock reflection, even though the shock approaches very close to the camber line. As a result, shock losses due to reflection are not accounted for, leading to a significantly lower entropy production compared to the CFD results. In the latter case, the blades have a finite thickness, and shock reflections actually occur. Furthermore, in this case the effect of the MP is also present. If the stator and rotor were evaluated separately (as in case A), the resulting efficiency would be 59.23%, roughly ten percentage points higher than in the full-stage configuration and much closer to the value predicted by the ML code.

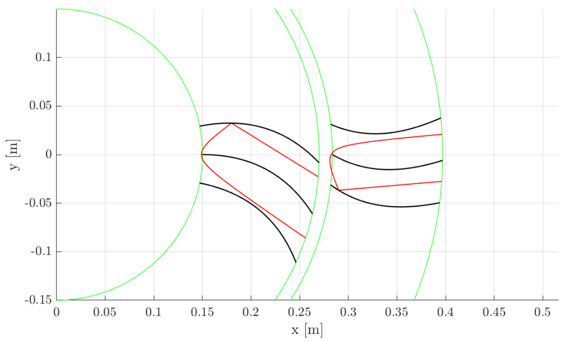

Figure 6: Shock pattern based on the camber lines predicted by the ML code for case D.

Metric	Unit	ML_D	CFD_D
η_{tt}	%	67.18	50.51
l_{eu}	kJ/kg	375.6	314.0
$\Delta s_{tot,MP}$	J/kgK	89.81	152.44
Δs_{stator}	J/kgK	44.85	53.01
Δs_{rotor}	J/kgK	44.96	68.39
M_1	-	2.154	2.094
M_{w2}	-	2.002	1.920
M_3	-	1.729	1.580
α_1	deg	41.35	39.80
β_2	deg	27.32	26.29
α_3	deg	0.488	4.119

Table 4: Comparison between ML and CFD results for case D.

4. Losses Breakdown

Although loss evaluation is particularly straightforward when using three-dimensional CFD sim-

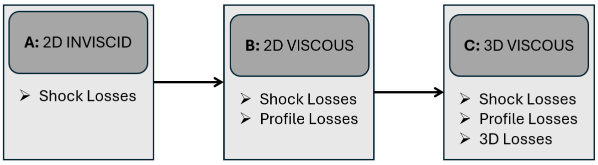

Figure 7: Qualitative scheme of the losses breakdown process.

ulations or experimental data, the same cannot be said for simplified methods such as ML approaches. For this reason, the concept of LB was thoroughly explored, in order to verify that the evaluation of the individual dissipation components associated with shock waves and profile losses is properly captured by the correlations adopted. To isolate the different loss mechanisms, the stator at the design point of Section 3.1 was analyzed under three different cases (see Figure 7):

- **A)** 2D simulation with slip boundary conditions on the blades: this case should contain information related solely to shock losses;
- **B)** 2D simulation with no-slip boundary conditions on the blades: this case should contain information related to shock and profile losses;
- **C)** 3D simulation with no-slip boundary conditions on the blades: this case should contain the same information as case B, together with any effects related to the 3D nature of the flow (such as secondary losses).

"Channel" refers to the entropy production from the inlet of the domain to the blade TE, whereas "mix" denotes the entropy production from the TE to the domain outlet.

The results of the analysis are reported in Tables 5 and 6.

	Case A	**Case B**	**Case C**
Δs_{tot}	58.35	67.76	67.78
$\Delta s_{\text{channel}}$	41.49	53.46	53.47
Δs_{mix}	16.86	14.30	14.31

Table 5: Entropy production for the three analyzed cases.

The losses associated with the shock within the passage amount to 41.49 J/kgK and can be compared with those obtained from the ML analysis (42.63 J/kgK). The profile losses were obtained

Loss Mechanism	Δs_{ML}	Δs_{LB}
Profile Losses	25.77	26.27
Shock Losses	42.63	41.49
Total Losses	68.40	67.78

Table 6: Comparison of entropy production between the ML and the LB analysis.

through:

$$\Delta s_{\text{prof}} = \Delta s^{B}_{\text{tot}} - \Delta s^{A}_{\text{chan}} = 26.27\; J/kgK \quad (3)$$

and are comparable with the value obtained using the Stewart method (25.77 J/kgK). The contributions of the profile losses associated with the channel and the mixing regions could be obtained by subtracting the results of Case A from those of Case B. As for case C, it is almost entirely identical to case B. This result was to be expected, since a slip condition was imposed along the endwall surfaces, limiting cross-flow gradients and therefore the onset of secondary or 3D phenomena. The outcome of the analysis is the possibility of cautiously adopting the LB concept, as well as the ability of the ML code to effectively predict loss production arising from the different contributions.

5. Conclusions

This work demonstrates the preliminary feasibility of a fully radial supersonic centrifugal turbine suitable for coupling with non-annular RDEs. The parametric analysis shows that the constraint associated with the formation of collective shocks restricts the operating domain, particularly for small geometries, and that efficiency increases with the work coefficient. The efficiency achieved at the design point is consistent with the supersonic nature of the flow and with the presence of internal shock systems within the channel. The ML model exhibits good predictive capability compared to CFD results, although limitations remain in the presence of collective shocks and in the accurate estimation of shock losses. Future developments include extending the ML code through more accurate deviation models, the treatment of SRG, the integration of dedicated blade design tools, and the inclusion of 3D effects such as endwall losses, in order to improve performance prediction. From a technological perspective, multi-variable optimization of the configuration represents the next step toward identifying the maximum-efficiency operating point.

6. Acknowledgements

This thesis was made possible thanks to the opportunity provided by Professor Paolo Gaetani, and to the invaluable guidance and support of Noraiz Mushtaq. I am also grateful for the academic and technical environment that allowed this work to be carried out successfully.

List of Symbols

Nomenclature

l_{eu}	Eulerian work
M	Mach number
s	Specific entropy
U	Peripheral velocity
V	Absolute velocity
W	Relative velocity
α	Absolute flow angle
β	Relative flow angle
η	Efficiency
λ	Work coefficient
φ	Flow coefficient

Subscripts

0	Stator inlet
1	Stator outlet
2	Rotor inlet
3	Rotor outlet
m	Meridional component
w	Relative quantity

Acronyms

LB	Losses Breakdown
LE	Leading Edge
ML	Meanline
MP	Mixing Plane
RDE	Rotating Detonation Engine
SRG	Stator-Rotor Gap
TE	Trailing Edge

References

[1] Piotr Wolański. Detonative propulsion. *Proceedings of the Combustion Institute*, 34:125–158, 2013.

[2] Warner L. Stewart. Analysis of two-dimensional compressible-flow loss characteristics downstream of turbomachine blade rows in terms of basic boundary-layer characteristics. Technical Report TN 3515, NACA, 1955.

[3] B. S. Stratford and G. S. Beavers. The calculation of the compressible turbulent boundary layer in an arbitrary pressure gradient: A correlation of certain previous methods. Reports and Memoranda ARC/R&M-3207, Aeronautical Research Council, Ministry of Aviation, 1959.

[4] W. E. Moeckel. Approximate method for predicting form and location of detached shock waves ahead of plane or axially symmetric bodies. Technical Note NACA TN-1921, National Advisory Committee for Aeronautics (NACA), 1949.

[5] Noraiz Mushtaq and Paolo Gaetani. Understanding and modeling unstarting phenomena in a supersonic inlet cascade. *Physics of Fluids*, 35(10):106101, 2023.